Summary:

Anatomy of active volcanic edifice at the Kusatsu-Shirane volcano, Japan, by magnetotellurics: hydrothermal implications for volcanic unrests

Tseng, K-H[1,2], Ogawa, Y.[2], Nurhasan[1,3], Tank, S.B.[1,4] , Ujihara, N.[1,5], Honkura, Y.[2], Terada, A.[2], Usui, Y.[1,6], Kanda, W.[2]

1: Department of Earth and Planetary Sciences, Tokyo Institute of Technology, Tokyo, Japan

2: Volcanic Fluid Research Center, Tokyo Institute of Technology, Tokyo, Japan

3: Physics Department, Bandung Institute of Technology, Bandung, Indonesia

4: Boğaziçi University, Kandilli Obs. & E.R.I., Çengelköy, İstanbul, Turkey

5: Hydrographic and Oceanographic Department, Japan Coast Guard, Tokyo, Japan

6: Earthquake Research Institute, The University of Tokyo, Tokyo, Japan

In this report, we briefly introduce the paper Tseng et al. (2020).

https://doi.org/10.1186/s40623-020-01283-2

Abstract

We aimed to perform three-dimensional imaging of the underlying geothermal system to a depth of 2 km using magnetotellurics (MT) at around the Yugama crater, the Kusatsu–Shirane Volcano, Japan, which is known to have frequent phreatic eruptions. We deployed 91 MT sites focusing around the peak area of 2 km × 2 km with typical spacings of 200 m. The full tensor impedances and the magnetic transfer functions were inverted, using an unstructured tetrahedral finite element code to include the topographic effect. The final model showed (1) low-permeability bell-shaped clay cap (C1) as the near-surface conductor, (2) brine reservoir as a deep conductor (C3) at a depth of 1.5 km from the surface, and (3) a vertical conductor (C2) connecting the deep conductor to the clay cap which implies an established fluid path. The columnar high-seismicity distribution to the east of the C2 conductor implies that the flushed vapor and magmatic gas was released from the brine reservoir by breaking the silica cap at the brittle–ductile transition. The past magnetization/demagnetization sources and the inflation source of the 2014 unrest are located just below the clay cap, consistent with the clay capped geothermal model underlain by brine reservoir. The resistivity model showed the architecture of the magmatic–hydrothermal system, which can explain the episodic volcanic unrest.

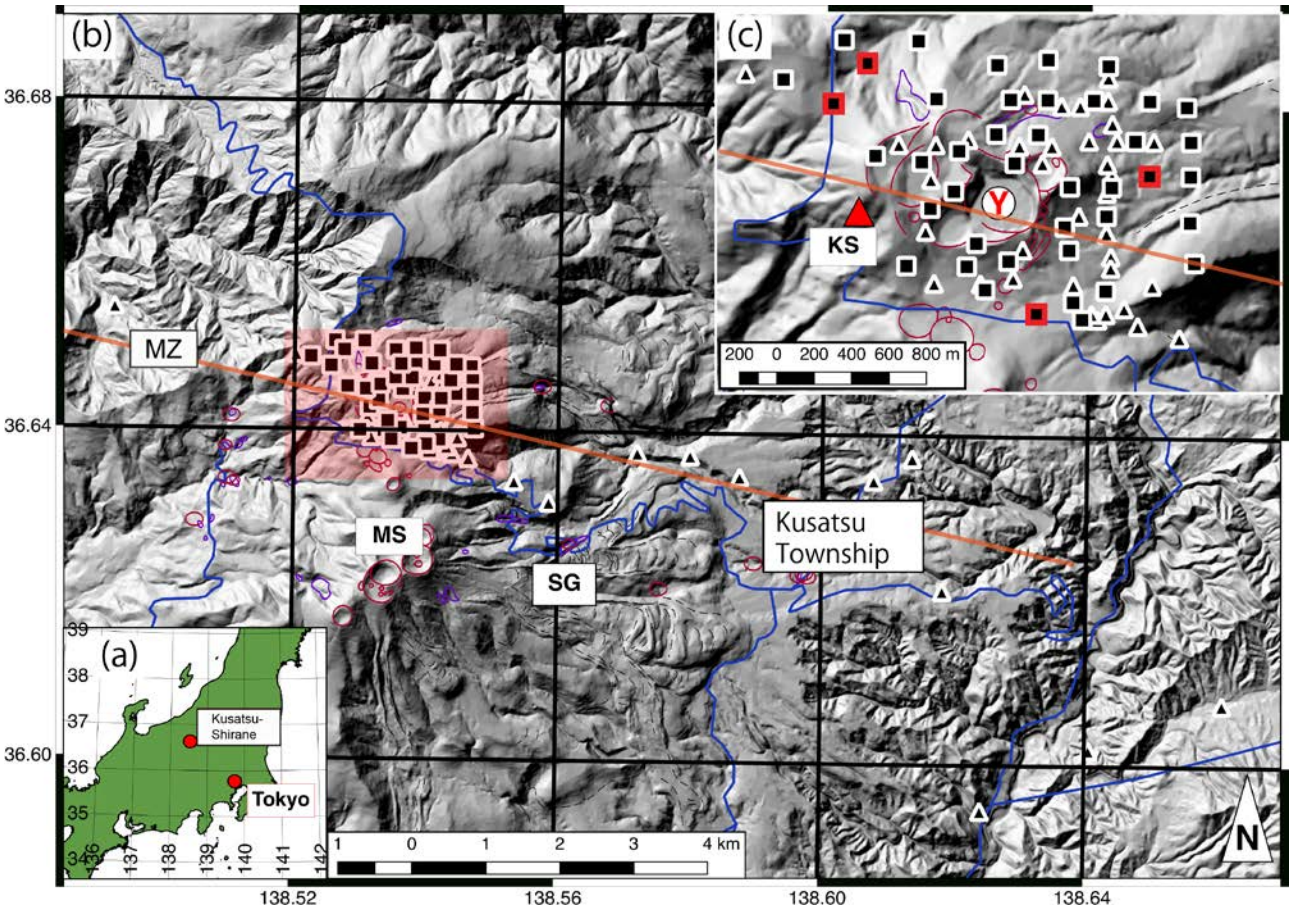

Fig.1

a Location of Kusatsu–Shirane Volcano, Japan.

b Topography map of Kusatsu–Shirane Volcano with MT/AMT stations. The squares and triangles denote the MT and AMT stations, respectively. The red circles and open curves show the crater rims of past eruptions. The purple closed curves show the fumarole zones. The blue curves show the national road 292 as a location reference. SG, MS, and MZ denote the locations of Sesshougawara fumarolic area, Mt. Motoshirane, and Manza hot spring field, respectively. The long orange line denotes the AMT profile (Nurhasan et al., 2006)

c A peak area [the red rectangle in (**b**)] of Kusatsu–Shirane Volcano with MT/AMT stations. The symbols are the same as in (**b**). Moreover, the black squares with red and with white edges denote the MT station with and without magnetic field data, respectively. KS denotes Mt. Shirane, and the red triangle denotes its peak. Y denotes the Yugama crater lake

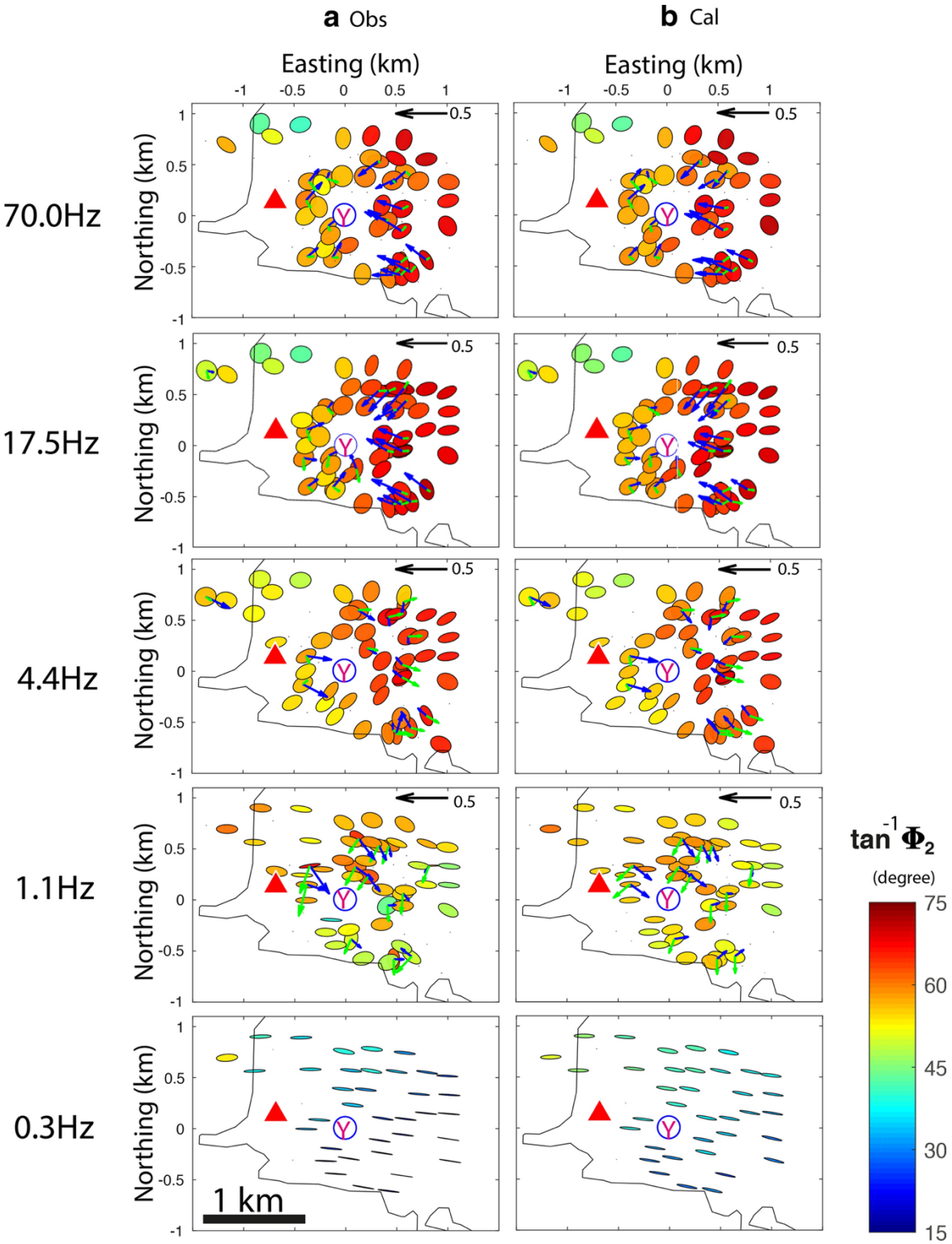

Fig.2 The phase tensor ellipses (Caldwell et al., 2004) map with **a** the observed and **b** the calculated data from the final model. The phase tensor ellipses are filled by $\tan^{-1}$ Φ2, where Φ2 is the geometric mean of maximum and minimum of phase tensor. The blue and green arrows show the real and imaginary parts of the induction vectors with Parkinson convention. The black curve, red triangle, and blue circle with Y denote the national road 292, the peak of Mt. Kusatsu–Shirane and the Yugama crater lake, respectively.

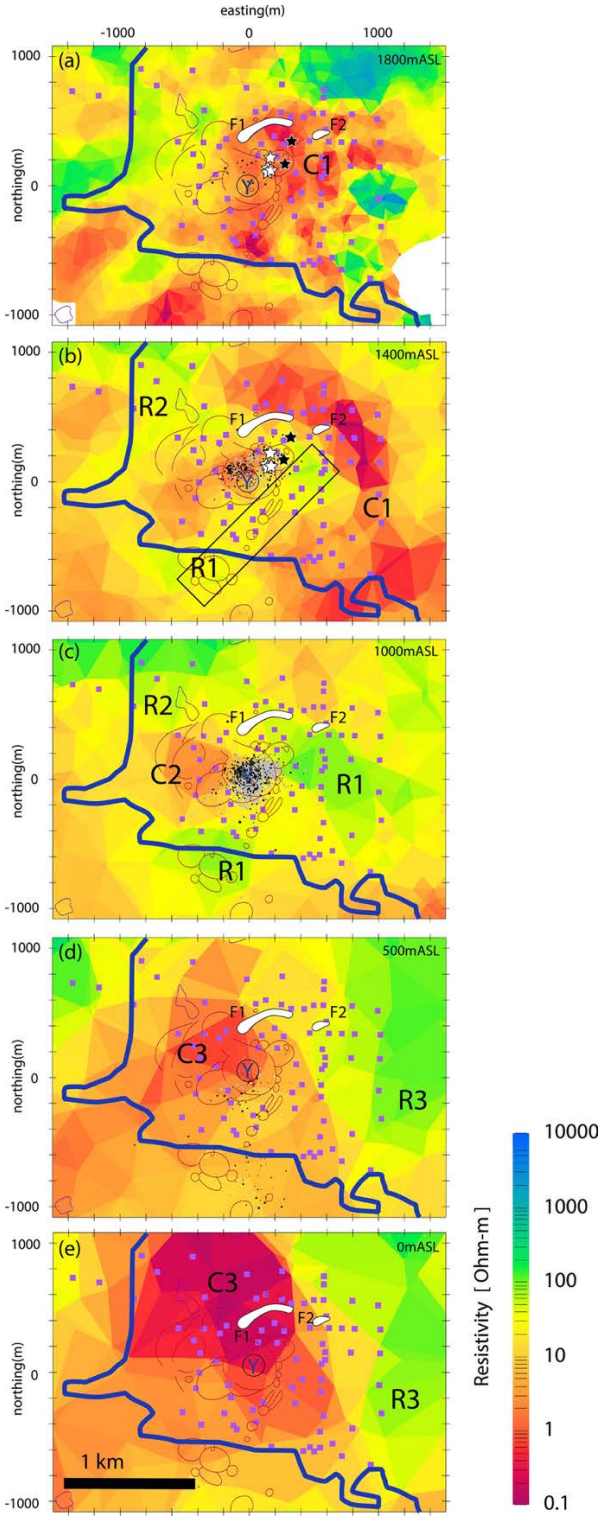

Fig. 3 Depth slices at **a** 1800 m ASL, **b** 1400 m ASL, **c** 1000 m ASL, **d** 500 m ASL and **e** 0 m ASL from the 3-D resistivity inversion at the peak area of Kusatsu–Shirane volcano using the unstructured tetrahedral code (Usui, 2015; Usui et al., 2017). Seismic hypocenters are mapped as dots on each map within 200 m tolerance in depth. The white, black, and gray dots denote hypocenters for three periods before, during and after the 2014 unrest, namely from August 2013 to February 2014, from March 2014 to May 2014, and from June 2014 to February 2019. The white and black starts denote horizontal locations of magnetizations and demagnetizations corresponding to volcanic events from 1978 to 2012 after Takahashi & Fujii (2014). The red circles and open curves show the crater rims of past eruptions. The rectangle in (b) denotes the fitting between the resistor R1 and the locations of historical eruptions. Major fumaroles (F1 and F2) are shown by white closed curves.

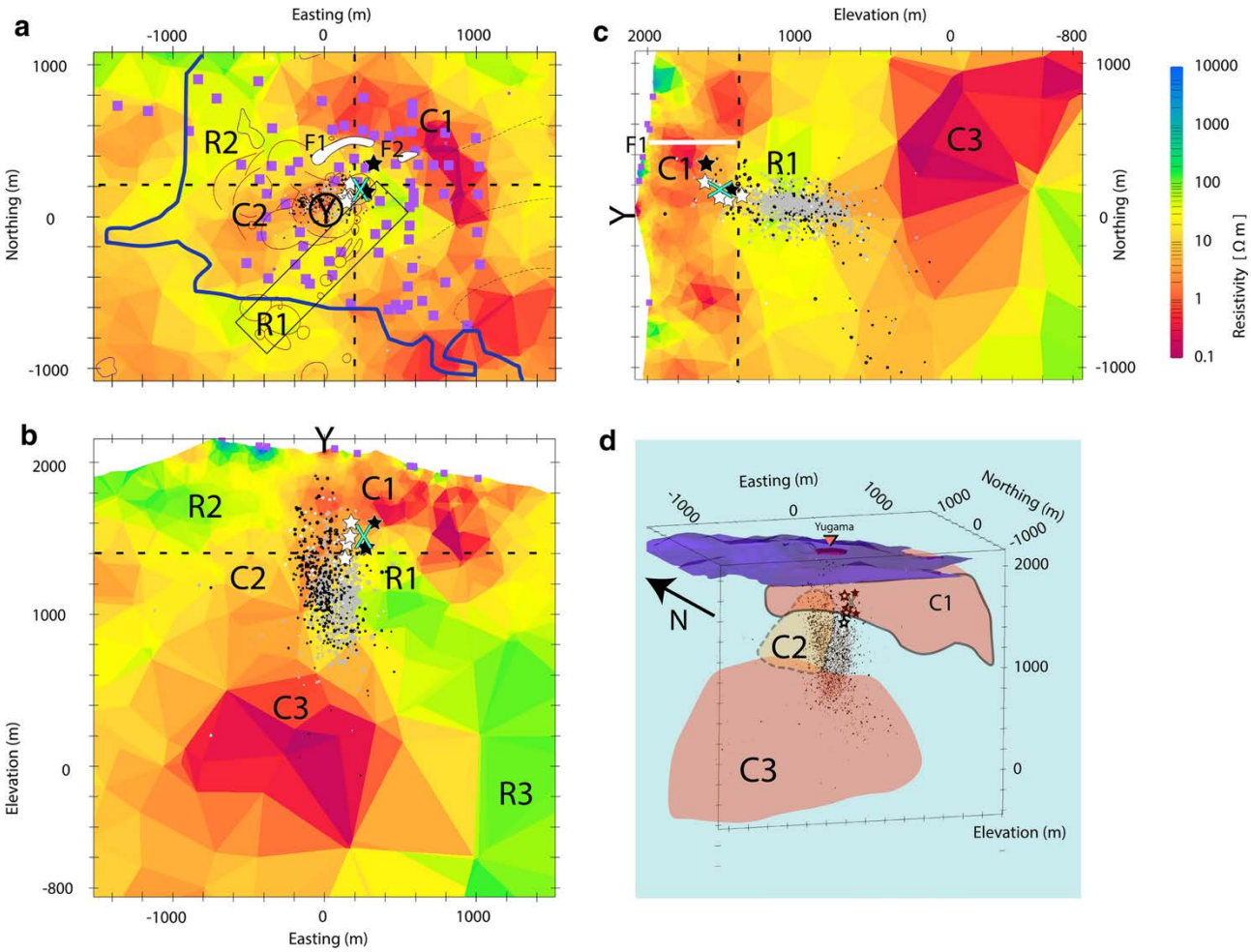

Fig.4

a Depth slice at 1400 m ASL. The locations for W–E and S–N profiles for sections are shown by broken lines.

b W–E and **c** S–N sections. The seismic hypocenters are mapped as dots on each map within 200 m tolerance normal to the sections. The white, black, and gray dots denote hypocenters before, during and after the 2014 unrest, respectively. The shallow seismicity (black dots) going through the clay cap (C1) is evident during 2014 unrest. The white and black stars denote the same as in Fig. 3. The blue X denote the point pressure

d The 3-D view of the three major conductors. The blue surface shows the topography. The dots denote seismicity as in (**a**–**c**).

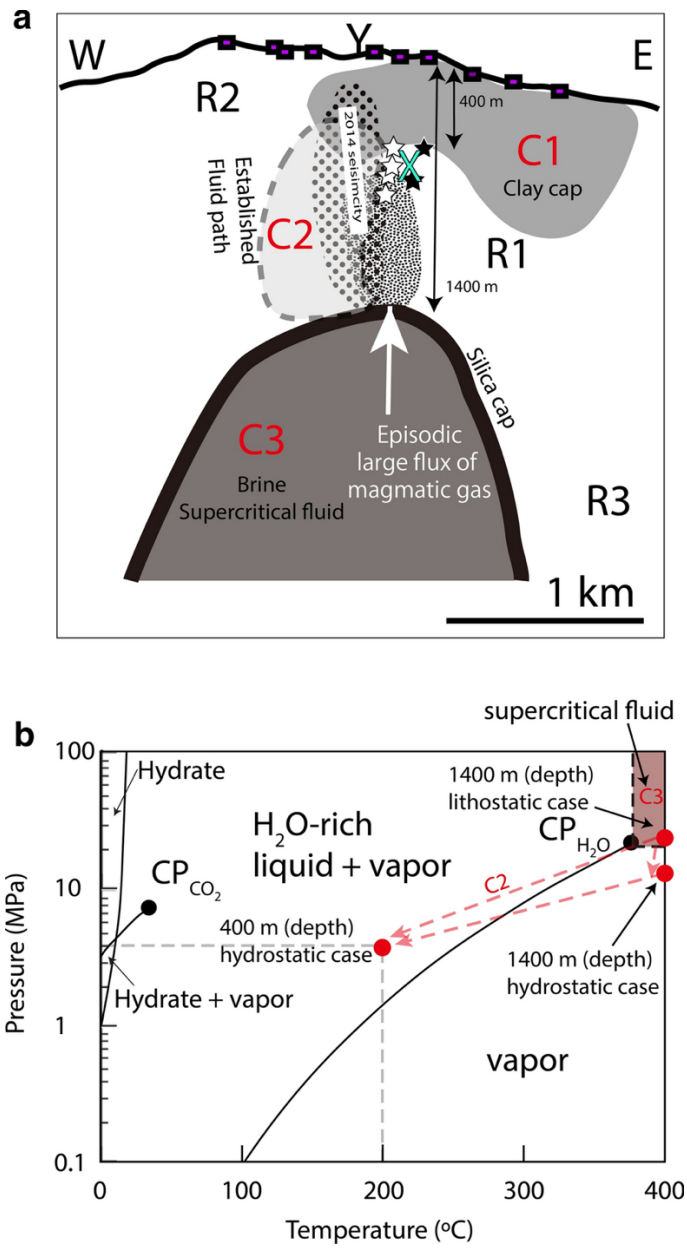

Fig. 5 a Simplified W–E resistivity section in Fig. 4b. The rectangles on the terrain denote the observation sites. The white and black stars and the green "X" symbols are the same as in Fig. 4. The swarm dots with bigger and with smaller circles denote the hypocenters of microseismic events during 2014 unrest, and out of this active period, respectively.

b Pressure–temperature projection of hydrothermal fluid phase diagram for H_2O and CO_2 (after Hutnak et al. 2009). Two curves which end with solid circles denote the liquid–vapor coexistence curves of pure CO_2 and pure H_2O with their critical points (CP). C2 may be an established fluid path from the supercritical fluid. In contrast, if episodic large gas flux breaks the silica cap (Fournier, 1999; Saishu et al., 2014), breakage of the silica cap over the brine (Afanasyev et al.,2018; Blundy et al. 2015) may flush the fluid upward in the hydrostatic domain.

References

Afanasyev A et al. (2018) Formation of magmatic brine lenses via focussed fluid-flow beneath volcanoes. Earth Planet Sci Lett 486:119–128. https://doi.org/10.1016/j.epsl.2018.01.013

Blundy J et al. (2015) Generation of porphyry copper deposits by gas–brine reaction in volcanic arcs. Nature Geosci 8:235–240. https://doi.org/10.1038/ngeo2351

Caldwell TG et al. (2004) The magnetotelluric phase ten- sor. Geophys J Int 158:457–469. https://doi.org/10.1111/j.1365- 246X.2004.02281.x

Fournier RO (1999) Hydrothermal processes related to movement of fluid from plastic into brittle rock in the magmatic–epithermal environment. Econ Geol 94:1193–1211. https://doi.org/10.2113/gsecongeo.94.8.1193

Hutnak M et al (2009) Numerical models of cal- dera deformation: effects of multiphase and multicomponent hydrother- mal fluid flow. J Geophys Res 114:B04411. https://doi.org/10.1029/2008J B006151

Nurhasan et al. (2006) Two electrical conductors beneath Kusatsu–Shirane volcano, Japan, imaged by audiomagnetotellurics, and their implications for the hydrothermal system. Earth Planets Space 58:1053–1059. https://doi. org/10.1186/BF03352610

Saishu H et al. (2014) The significance of silica precipi- tation on the formation of the permeable–impermeable boundary within Earth's crust. Terra Nova 26:253–259. https://doi.org/10.1111/ ter.12093

Takahashi K, Fujii I (2014) Long-term thermal activity revealed by magnetic measurements at Kusatsu–Shirane volcano, Japan. J Volcanol Geotherm Res 285:180–194. https://doi.org/10.1016/j.jvolgeores.2014.08.014

Tseng, K.H. et al. (2020), Anatomy of active volcanic edifice at the Kusatsu–Shirane volcano, Japan, by magnetotellurics: hydrothermal implications for volcanic unrests. *Earth Planets Space* **72,** 161

Usui Y (2015) 3-D inversion of magnetotelluric data using unstructured tetra- hedral elements: applicability to data affected by topography. Geophys J Int 202:828–849. https://doi.org/10.1093/gji/ggv186

Usui Y et al. (2017) Three-dimensional resistivity structure of Asama Volcano revealed by data-space magnetotelluric inversion using unstruc- tured tetrahedral elements. Geophys J Int 208:1359–1372. https://doi. org/10.1093/gji/ggw459